Contrasting the responses of three different ground-based instruments to energetic electron precipitation

Craig J. Rodger,[1] Mark A. Clilverd,[2] Andrew J. Kavanagh,[3] Clare E. J. Watt,[4] Pekka T. Verronen,[5] and Tero Raita[6]

Received 12 December 2011; revised 27 February 2012; accepted 13 March 2012; published 25 April 2012.

[1] In order to make best use of the opportunities provided by space missions such as the Radiation Belt Storm Probes, we determine the response of complementary subionospheric radiowave propagation measurements (VLF), riometer absorption measurements, cosmic noise absorption, and GPS-produced total electron content (vTEC) to different energetic electron precipitation (EEP). We model the relative sensitivity and responses of these instruments to idealized monoenergetic beams of precipitating electrons, and more realistic EEP spectra chosen to represent radiation belts and substorm precipitation. In the monoenergetic beam case, we find riometers are more sensitive to the same EEP event occurring during the day than during the night, while subionospheric VLF shows the opposite relationship, and the change in vTEC is independent. In general, the subionospheric VLF measurements are much more sensitive than the other two techniques for EEP over 200 keV, responding to flux magnitudes two-three orders of magnitude smaller than detectable by a riometer. Detectable TEC changes only occur for extreme monoenergetic fluxes. For the radiation belt EEP case, clearly detectable subionospheric VLF responses are produced by daytime fluxes that are ~10 times lower than required for riometers, while nighttime fluxes can be 10,000 times lower. Riometers are likely to respond only to radiation belt fluxes during the largest EEP events and vTEC is unlikely to be significantly disturbed by radiation belt EEP. For the substorm EEP case both the riometer absorption and the subionospheric VLF technique respond significantly, as does the change in vTEC, which is likely to be detectable at ~3–4 total electron content units.

Citation: Rodger, C. J., M. A. Clilverd, A. J. Kavanagh, C. E. J. Watt, P. T. Verronen, and T. Raita (2012), Contrasting the responses of three different ground-based instruments to energetic electron precipitation, *Radio Sci.*, *47*, RS2021, doi:10.1029/2011RS004971.

1. Introduction

[2] The basic structure of the Van Allen radiation belts was recognized from shortly after their discovery following the International Geophysical Year [*Van Allen and Frank*, 1959; *Hess*, 1968; *Van Allen*, 1997]. However, despite being discovered at the dawn of the space age, there are still fundamental questions concerning the acceleration and loss of highly energetic electrons [*Reeves et al.*, 2009; *Thorne*, 2010] in the radiation belts. Energetic electron fluxes can increase or decrease by several orders of magnitude on time scales less than a day [e.g., *Morley et al.*, 2010]. In response to these questions NASA's Living with a Star Radiation Belt Storm Probe (RBSP) mission is scheduled for launch in mid-late 2012 and may be accompanied by several other dedicated radiation belt missions (e.g., the USAF DSX, the Russian RESONANCE mission and Japan's ERG).

[3] Supporting these major space-based investigations, multiple researchers and groups are planning near Earth measurements which will focus upon the loss of energetic electrons into the atmosphere. These range from new campaigns flowing from the Living With a Star Mission of Opportunity program (i.e., BARREL [*Millan and the BARREL Team*, 2011]) through to existing ground-based observatories who have expanded their coverage in preparation for the RBSP mission (e.g., AARDDVARK [*Clilverd et al.*, 2009]).

[4] The coupling of the Van Allen radiation belts to the Earth's atmosphere through precipitating particles is an area of intense scientific interest, principally due to two separate research activities. One of these concerns the physics of the radiation belts, and primarily the evolution of energetic electron fluxes during and after geomagnetic storms [e.g., *Reeves et al.*, 2003]. The other focuses on the response of the atmosphere to precipitating particles, with a possible linkage to climate variability [e.g., *Turunen et al.*, 2009; *Seppälä*

[1]Department of Physics, University of Otago, Dunedin, New Zealand.
[2]British Antarctic Survey, National Environment Research Council, Cambridge, UK.
[3]Department of Physics, Lancaster University, Lancaster, UK.
[4]Department of Physics, University of Alberta, Edmonton, Alberta, Canada.
[5]Finnish Meteorological Institute, Helsinki, Finland.
[6]Sodankylä Geophysical Observatory, University of Oulu, Sodankylä, Finland.

0048-6604/12/2011RS004971

et al., 2009]. Both scientific areas require increased understanding of the nature of the precipitation, particularly with regards to the precipitation drivers, as well as the variation of the flux and energy spectrum for electrons lost from the outer radiation belts.

[5] Essentially all geomagnetic storms substantially alter the electron radiation belt populations via acceleration, loss and transport processes [*Reeves et al.*, 2003, 2009] where precipitation losses in to the atmosphere play a major role [*Green et al.*, 2004; *Millan and Thorne*, 2007]. A significant fraction of all of the particles lost from the radiation belts are precipitated into the atmosphere [*Lorentzen et al.*, 2001; *Horne*, 2002; *Friedel et al.*, 2002; *Clilverd et al.*, 2006], although storm-time non-adiabatic magnetic field changes also lead to losses through magnetopause shadowing [e.g., *Ukhorskiy et al.*, 2006].

[6] The impact of precipitating particles on the environment of the Earth is also an area of recent scientific focus. Precipitating charged particles produce odd nitrogen and odd hydrogen in the Earth's atmosphere which can catalytically destroy ozone [*Brasseur and Solomon*, 2005]. As a result, energetic electron precipitation (EEP) events have been linked to significant decreases in polar ozone in the upper stratosphere [e.g., *Randall et al.*, 2007; *Seppälä et al.*, 2007]. By influencing stratospheric ozone variability, energetic particle precipitation can affect the stratospheric radiative balance, and may link to climate variability [*Rozanov et al.*, 2005; *Seppälä et al.*, 2009]. Recent experimental studies have demonstrated the direct production of odd nitrogen [*Newnham et al.*, 2011] and odd hydrogen [*Verronen et al.*, 2011; M. Andersson et al., Precipitating radiation belt electrons and the production of mesospheric hydroxyl during 2004–2009, submitted to *Journal of Geophysical Research*, 2011] in the mesosphere by EEP during geomagnetic storms.

[7] In order to make best use of the opportunities provided by space missions such as RBSP it is important to understand the response of extensive ground-based instrumentation networks to different EEP characteristics. In this paper we focus upon subionospheric VLF propagation measurements, riometers (relative ionospheric opacity meter) absorption measurements, and GPS derived total electron content. In particular, we aim to contrast the predicted sensitivity and responses of these instruments to monoenergetic beams of precipitating electrons, EEP from the radiation belts, and EEP during substorms. Recent work has demonstrated that both geomagnetic storms and substorms produce high levels of EEP [e.g., *Rodger et al.*, 2007; *Clilverd et al.*, 2008, 2012], and can significantly alter mesospheric neutral chemistry [*Rodger et al.*, 2010; *Newnham et al.*, 2011]. Networks of multiple precipitation sensing ground-based instruments exist for each of our three selected techniques, for example the AARDDVARK array of subionospheric radio receivers [*Clilverd et al.*, 2009], the GLORIA riometer array [*Alfonsi et al.*, 2008], and the Canadian High Arctic Ionospheric Network (CHAIN) of GPS receivers [*Jayachandran et al.*, 2009].

2. Modeling of Electron-Density Produced Ionization Changes

[8] Figure 1 shows a schematic of the ground-based instruments we consider in the current study. Subionospheric radio receivers detect precipitation due to changes in the ionization number density around the lower *D* region boundary. As VLF waves propagate beneath the ionosphere in the Earth-ionosphere waveguide, any change in the height of the *D* region boundary will produce changes in the received amplitude and phase. Due to the low attenuation of VLF subionospheric propagation, the EEP-modified ionospheric region may be far from the transmitter or the receiver and a combination of ionospheric and electromagnetic wave modeling must be invoked to constrain where the EEP has modified the ionosphere. In contrast, riometers observe local EEP-produced changes occurring directly above the instrument. In this case the increased ionization number density in the *D* and *E* regions, due to EEP, results in the absorption of the HF "cosmic noise" passing through the ionosphere. Finally, the signals arriving at GPS receivers can be used to determine the total electron content (TEC) as the navigation signals pass through the entire ionosphere from the satellite to the receiver. Signals from satellites closest to the ground receiver can be easily converted to vertical TEC (vTEC) under the assumption of a thin ionosphere, and are therefore again a "local" measurement. Generally, vTEC measurements are dominated by the ionospheric *F* region and the changes which occur in those altitudes [*Mendillo*, 2006]. However, a recent paper has argued that substorm-driven EEP can lead to significant vTEC changes due to modification of the ionospheric *D* and *E* regions [*Watson et al.*, 2011], leading to the inclusion of this technique in our study.

2.1. Riometers

[9] The riometer utilizes the absorption of cosmic radio noise by the ionosphere [*Little and Leinbach*, 1959] to measure the enhancement of *D* region electron concentration caused by EEP. The riometer technique compares the strength of the cosmic radio noise signal received on the ground to the normal sidereal variation referred to as the absorption quiet-day curve (QDC) to produce the change in cosmic noise absorption (ΔCNA). The cosmic radio noise propagates through the ionosphere and part of the energy is absorbed due to the collision of the free ionospheric electrons with neutral atmospheric atoms. The instantaneous ionospheric absorption in decibels is derived from the ratio of the prevailing signal level to this curve [*Krishnaswamy et al.*, 1985]. Typically the absorption peaks near 90 km altitude, where the product of electron density and neutral collision frequency maximizes. Simple expressions for the absorption of cosmic radio noise (A) can be derived from the Appleton-Hartree equations [e.g., *Nyland*, 2007],

$$A = 4.61 \times 10^{-5} \int_{h_1}^{h_2} \left[\frac{N_e(h) \cdot \upsilon_{en}(h)}{\upsilon_{en}^2(h) + (2\pi f \pm \omega_{Be})^2} \right] dh \ [\mathrm{dB}] \qquad (1)$$

where

A absorption (power absorbed on propagation through the ionosphere) with units of dB;

N_e height dependent electron number density profile with units of electrons per cubic meter;

υ_{en} dependent effective electron-neutral collision profile (collisions per second) which can be taken from the empirical fitting of *Rodger et al.* [1998];

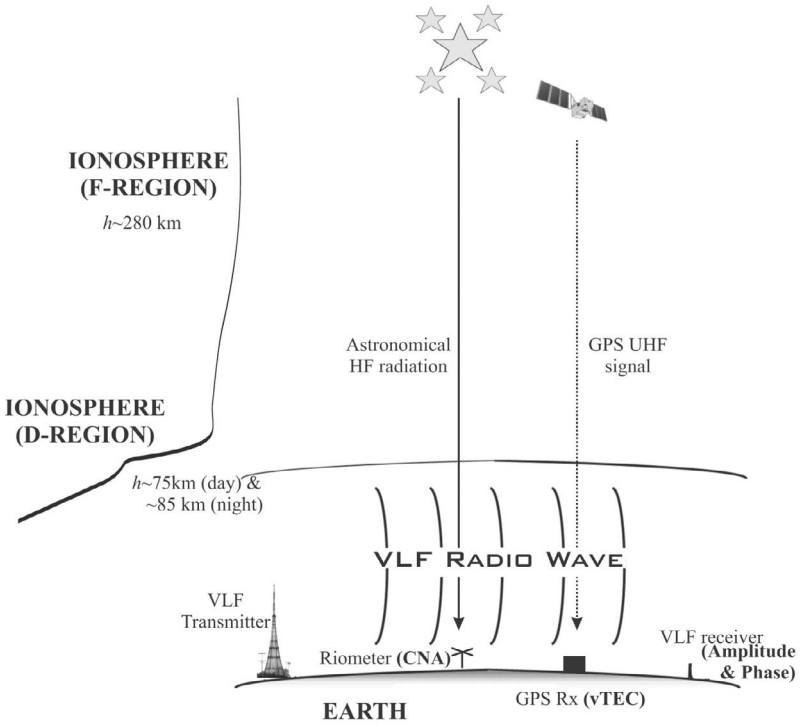

Figure 1. Schematic of the ground-based instruments considered in the current study. Subionospheric VLF propagation detects precipitation due to changes in the ionization number density around the lower *D* region boundary, as the VLF waves propagate beneath the ionosphere. Riometers observe increases in the absorption of "cosmic noise" produced due to increases in the ionization number density in the *D* and *E* regions. GPS receivers can measure the vertical total electron content (vTEC) as the navigation signals pass through the entire ionosphere.

f frequency of the cosmic radio noise (in Hz);
ω_{Be} electron gyrofrequency.

[10] Integration of expression (1) through a height dependent ionosphere produces the absorption for a given electron density profile for each of the two modes (O and X, respectively). After subtracting the absorption for an ambient or undisturbed electron density profile (that is one with no EEP flux) to represent the absorption QDC conditions the change in CNA can be calculated (i.e., ΔCNA), which in practice is the quantity of interest. However, care must be taken as to the inclusion of the two modes (A_O and A_X). Imaging riometers (IRIS instruments) are large receiver arrays which measure only the X-mode but provide an image of the CNA above the instrument [*Detrick and Rosenberg*, 1990]. However, many researchers make use of "simple" wide-beam Yagi riometer instruments, which respond to both modes. It is common to take the mean of the two modes to represent the total CNA [e.g., *Friedrich et al.*, 2002]. This is a reasonable approximation to the total absorption (A_T):

$$A_T = \frac{2A_X A_O}{A_X + A_O} \text{ [dB]} \tag{2}$$

For a typical 30 MHz riometer the ratio of A_X and A_O will be about 1.25 such that A_T will be approximately 1.11 A_O. The arithmetic mean of the absorption quantities A_X and A_O is 1.125 A_O. Thus, in many cases the arithmetic mean should be a reasonable approximation of the total absorption, as the instrumental sensitivity will be about 0.1 dB (with the uncertainty in the QDC being of the same order).

[11] For the calculations presented below we will assume a 30 MHz wide-beam riometer.

2.2. Subionospheric VLF

[12] This technique senses changes in the subionospheric waveguide formed by the lower ionospheric boundary in the *D* region and the conducting ground (land, sea, or ice). The upper boundary of the waveguide is the ionized *D* region at ~70–85 km, and varies due to local increases in ionization rates caused by EEP penetrating to altitudes below the *D* region boundary. These local changes produce changes in the received amplitude and phase at the receiver system, which may be thousands of kilometers "downstream" from where the EEP strikes the ionosphere. The EEP causes the base of the ionosphere to decrease and thus changes the propagation of the waveguide modes, resulting in a change in the received signal. However, as the received wave is a combination of all the available modes the amplitude may increase or decrease, and the phase advance or retard, depending on the combination of the modes.

[13] During undisturbed conditions the amplitude and phase of fixed frequency VLF transmissions varies in a consistent way and thus EEP events can be detected as deviations from the subionospheric "quiet day curve" producing a change in received amplitude (ΔAmplitude) and phase (ΔPhase), relative to the QDC–here QDC refers to diurnal variation in received VLF amplitude and phase

rather than a CNA. Due to interference between the modes and the strong differences in the *D* region reflection altitudes between day and night, the subionospheric QDC tends to have a complex form but is highly reproducible [e.g., *Clilverd et al.*, 1999] albeit with more variation from night to night than from day to day. For a much more comprehensive review of this topic we refer the reader to the discussion by *Barr et al.* [2000] which highlights the development of VLF radio wave propagation measurements particularly over the last 50 years. Additional discussions on the use of subionospheric VLF propagation to sense space weather-produced changes can be found in the work by *Clilverd et al.* [2009]. Uncertainties in subionospheric VLF QDC will depend upon the time of day, the receiver design and the background noise levels. As an example, one EEP-study which relied upon subionospheric VLF concluded there was a ±0.3 dB amplitude uncertainty as a result of removing the subionospheric QDC at noon time and a ±1 dB amplitude uncertainty at nighttime [*Rodger et al.*, 2007].

[14] In order to interpret any observed fluctuations in a received VLF signal it is necessary to reproduce the characteristics of the deviations using mathematical descriptions of VLF wave propagation, and thus determine the ionization changes that have occurred around the upper waveguide boundary. In the current study we make use of the U.S. Navy Long Wave Propagation Code (LWPC) [*Ferguson and Snyder*, 1990] which models VLF signal propagation from any point on Earth to any other point. The code models the variation of geophysical parameters along the path as a series of horizontally homogeneous segments. To do this, the program determines the ground conductivity, dielectric constant, orientation of the geomagnetic field with respect to the path and the solar zenith angle, at small fixed-distance intervals along the path. Given electron density profile parameters for the upper boundary conditions for each section along the path, LWPC calculates the expected amplitude and phase of the VLF signal at the reception point.

2.3. GPS Determined TEC

[15] The absolute total electron content (TEC) can be estimated from the range delay of two radio signals with different frequencies propagating through the low-altitude magnetosphere and ionosphere between a GPS satellite and a ground station. Absolute TEC is obtained from the pseudoranges P_1 and P_2 for GPS frequencies f_1 = 1575.42 MHz and f_2 = 1227.60 MHz [*Skone*, 2001]:

$$\mathrm{TEC} = \frac{1}{40.3}\left(\frac{1}{f_1^2}-\frac{1}{f_2^2}\right)^{-1}(P_1 - P_2 - b_\mathrm{r} - b_\mathrm{s}), \qquad (3)$$

where b_r and b_s are the receiver and satellite interchannel bias terms, respectively. The uncertainty in absolute TEC can be between 1 and 5 TECu (where 1 TECu = 10^{16} electrons m^{-2}) due to receiver or satellite biases and multipath effects.

[16] Relative changes in TEC can be estimated using the carrier phase ranges Φ:

$$\mathrm{TEC} = -\frac{1}{40.3}\left(\frac{1}{f_1^2}-\frac{1}{f_2^2}\right)^{-1}(\Phi_1 - \Phi_2), \qquad (4)$$

assuming that the ambiguities in the signal phase are relatively constant in time. These relative variations have much greater accuracy, ~0.10 TECu [*Skone*, 2001].

[17] The above estimates provide TEC, or relative changes in TEC, along the entire raypath between satellite to station, and further assumptions must be made to estimate the vertical TEC (vTEC) directly upward above the ground station. Typically, the estimated TEC is projected to the local zenith direction to obtain the vertical TEC using a mapping function $M(\varepsilon)$ that models the ionosphere as a uniform thin shell with a well-defined average height h [e.g., *Arikan et al.*, 2003]:

$$M(\varepsilon) = \left[1 - \left(\frac{R_E \cos(\varepsilon)}{R_E + h}\right)^2\right]^{-1/2} \qquad (5)$$

where R_E is the Earth radius, and ε is the elevation angle of the satellite measured at the receiver. vTEC can be easily compared with model predictions since it is the equivalent of the height-integrated electron number density through the ionosphere [e.g., *Anderson et al.*, 1987]:

$$\text{vertical TEC} = 10^{-16}\int_{h_1}^{h_2} N_e(h)\ dh\ [\mathrm{TECu}]. \qquad (6)$$

[18] In this study we will consider the change in vTEC with and without the addition of EEP, which we will define as ΔvTEC.

2.4. EEP-Produced Changes in Electron Number Density

[19] In order to estimate the response of the various instruments to EEP, we start by determining the change in ionospheric electron number density over the altitude range 40–150 km caused by precipitation. This altitude range covers the altitudes of peak energy deposition for electrons with energies from about 1 keV to 10 MeV, which is sufficient for our EEP study. The ambient, or undisturbed electron density profile, is provided by the International Reference Ionosphere (IRI-2007) (online from http://omniweb.gsfc.nasa.gov/vitmo/iri_vitmo.html) for the equinox on 21 March at 18 UT for "day" conditions and 6 UT for night, with the "STORM" model switched off. As the IRI does not include all of the *D* region, particularly during the nighttime, we combine the IRI results with typical *D* region electron density profiles determined for high latitudes at noon [*Thomson et al.*, 2011] and for nighttime conditions [*Thomson and McRae*, 2009].

[20] For the purposes of the modeling we will first focus on the location of Island Lake (53.86°N, 265.34°E, L = 5.2), Canada, marked by the yellow square in Figure 2. This site hosts a NORSTAR riometer and lies close to the midpoint of the great circle path from the VLF transmitter NDK (green circle, North Dakota, 25.2 kHz) and the AARDDVARK VLF receiver at Churchill (58.75°N, 265.1°E, L = 7.6). While we could select any location for our essentially theoretical comparisons, the point we have chosen provides the advantage of being applicable to the real world. In later sections, we will use other sites in order to compare directly with observations during particular events.

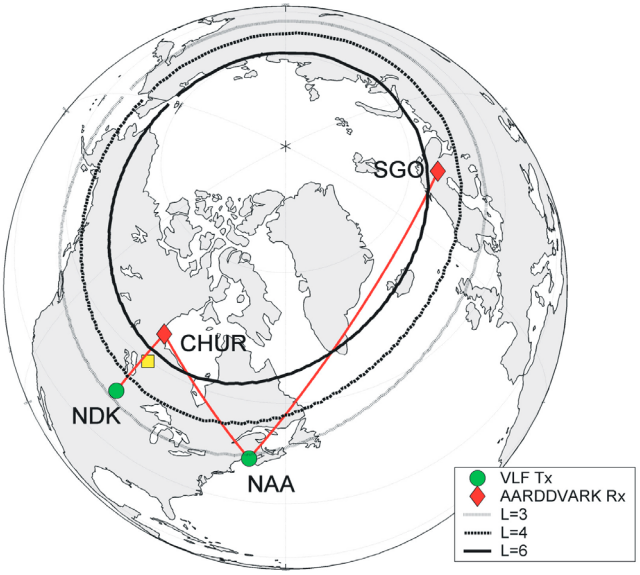

Figure 2. Map showing the location of the modeling point (yellow square), the AARDDVARK receivers at Churchill and Sodankylä (red diamonds) and the VLF transmitter NDK and NAA (green circles). This map also indicates the great circle propagation paths between the transmitter and receiver, as well as a number of fixed *L*-shell contours evaluated at 100 km altitude.

[21] The ionization rate due to precipitating energetic electrons is calculated by an application of the expressions in the work by *Rees* [1989], expanded to higher energies based on *Goldberg et al.* [1984]. The background neutral atmosphere is calculated using the NRLMSISE-00 neutral atmospheric model [*Picone et al.*, 2002]. The equilibrium electron number density in the lower ionosphere, is provided by a simplified ionospheric model [*Rodger et al.*, 1998, 2007] that has been expanded to encompass a wider range of altitudes and ionization rates. The Sodankylä Ion and Neutral Chemistry model (SIC) [*Verronen et al.*, 2005] was run for daytime and nighttime conditions with height-independent, non-varying ionization rates (i.e., ionization rates that were constant from 40 to 150 km altitude). Empirical weighting factors to the earlier equilibrium electron number density model were determined to best reproduce the SIC calculations. The results of this are shown in Figure 3 where the solid curves show the electron number density profiles generated by the SIC model, and the dashed curves are the result of the simplified equilibrium electron density model. There is very good agreement between the two models for a very wide range of ionization rates over the EEP-relevant altitude range. In practice the ionization rate is not constant with altitude, and maximizes at an altitude dependent upon the electron energy [*Turunen et al.*, 2009, Figure 3], at least for monoenergetic beam. Note that the same altitude-constant ionization rate will lead to a larger electron number density during the day than during the night (although the relative change may well be larger due to the comparatively weak nighttime ionosphere). Physically, this is due to photo-detachment of electrons which had attached to neutral forming a negative ion. During the night this can be a significant loss mechanism for free electrons, but during the day attachment to neutrals is effectively less efficient due to the competing photo-detachment process.

3. Monoenergetic EEP Beams

[22] In Figure 4 we consider the modeled response of the three EEP-sensing techniques to monoenergetic electrons precipitating into the upper atmosphere. While this is not a realistic representation of EEP from the radiation belts or during substorms, it is instructive as a comparison of the relative sensitivities of the three observation techniques. As

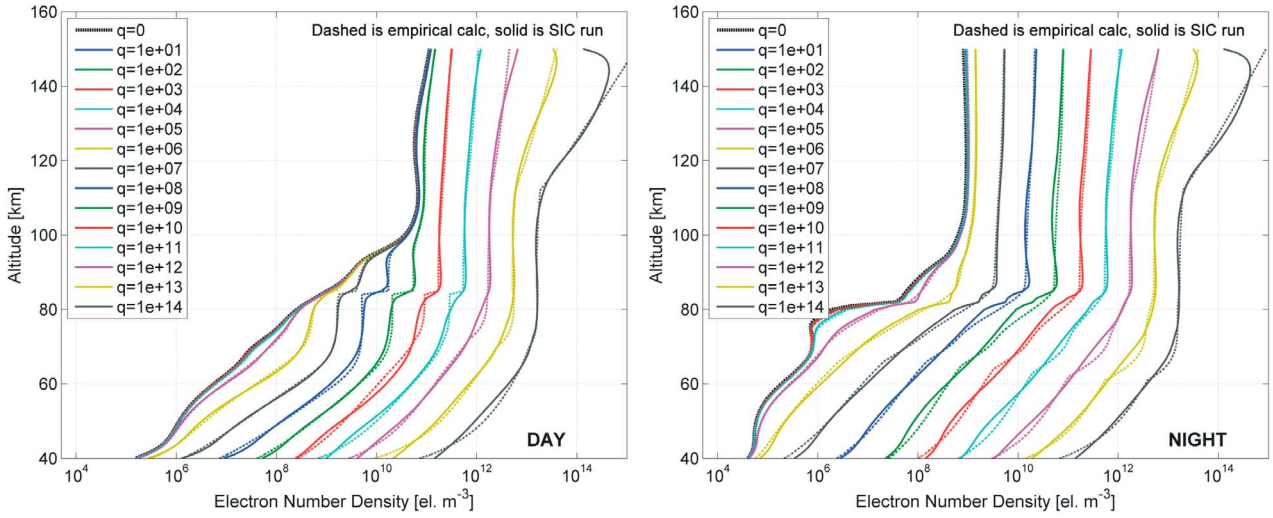

Figure 3. Electron number density calculations undertaken for ionization rates (q [electrons m^{-3}]) which were constant with altitude for (left) day and (right) night onditions. The solid curves are the results from the Sodankylä Ion and Neutral Chemistry (SIC) model, while the dashed curves are from an equilibrium electron density model which has been fitted to the SIC results. Note that the curves for $q < 10^4$ electrons m^{-3}, are almost indistinguishable on this plot from the electron number density for $q = 0$.

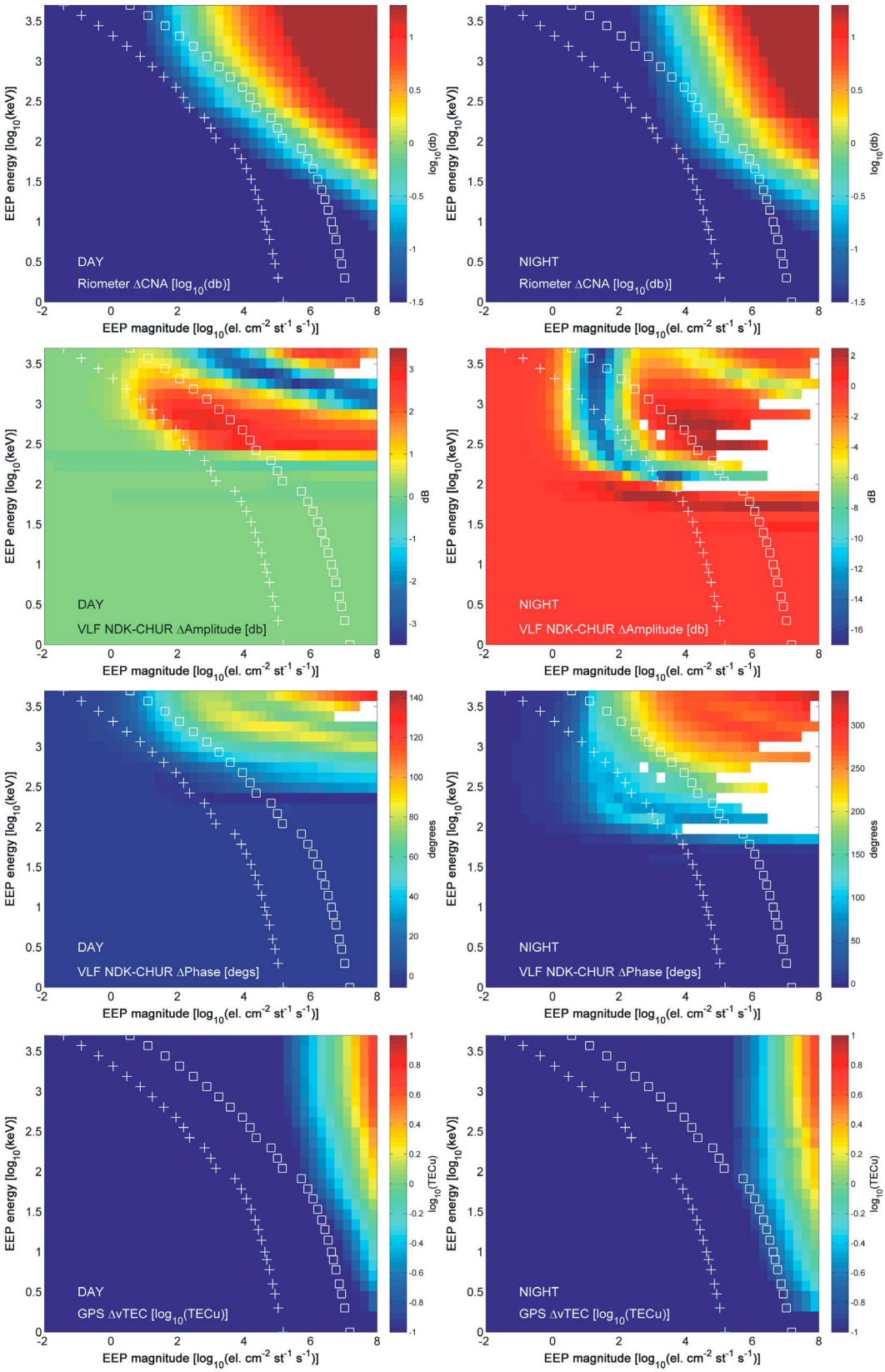

Figure 4. The varying response of the three EEP-sensing techniques to monoenergetic electrons precipitating into the upper atmosphere. White crosses represent an extreme EEP flux, where the entire ESA-SEE1 model tube population is precipitated in 10 min, while the white squares are the highly extreme storm-time case with 10^2 larger EEP magnitudes.

noted earlier, we allow for a wide range of EEP energies, spanning from 1 keV to 10 MeV, and take a similarly wide range of precipitation flux magnitudes, from 10^{-2} electrons cm^{-2} st^{-1} s^{-1} to 10^{8} electrons cm^{-2} st^{-1} s^{-1}. The upper energy range is an extreme estimate of precipitation flux for any reasonable radiation belt EEP event, and corresponds to the approximate flux used to represent 5 keV "auroral" electron precipitation by *Turunen et al.* [2009, Figure 5]. In order to provide bounds for a realistic range of possible EEP flux levels, Figure 4 includes white crosses to show the maximum precipitating flux, calculated by assuming the entire electron flux stored in a L = 5.3 flux tube can be precipitated out in a 10 min period, calculated using the ESA-SEE1 radiation belt model [*Vampola*, 1997]. During storms the trapped population of the radiation belts can be boosted by several orders of magnitude, and so these higher flux levels are indicated using white squares, representing a very extreme storm time case in which EEP fluxes are 100 times larger than the typical flux tube populations provided by the radiation belt model. Note however, that clearing the entire electron population of a flux tube in 10 min should be regarded as a very extreme example of radiation belt loss.

[23] The upper ionosphere electron density profile changes were calculated as outlined in section 2.4, after which the response of each instrument to the ionospheric change was estimated for a sunlit ionosphere (Figure 4, left) and a nighttime ionosphere (Figure 4, right). The first row in Figure 4 presents the calculations of the riometer ΔCNA, the second and third rows present the change in amplitude and phase for the subionospheric VLF propagation case from NDK to Churchill, and the fourth row presents the GPS derived ΔvTEC. For the subionospheric VLF propagation, the precipitation is introduced on the section of the great circle path which lies from 0.16 to 1.28 Mm from the NDK transmitter, corresponding to L = 3.5–7, i.e., a reasonable range for the outer radiation belt. The colorscale has been limited to reflect an estimated minimum detectable instrumental change of ∼0.05 dB for a riometer and 0.1 TECu for the GPS vTEC measurement. We have imposed a ceiling of 20 dB on the riometer response to reflect an approximate maximum "real world" value. The maximum modeled ΔCNA value of ∼1960 dB is unrealistic. For subionospheric VLF propagation the LWPC calculations fails in some cases, which are shown in white in Figure 4.

[24] Figure 4 demonstrates that the three EEP-sensing techniques have different threshold flux magnitudes and electron energies that allow the detection of EEP, as well as different responses to day and night ambient conditions. For techniques which rely upon electromagnetic radiation passing through the ionosphere, such as riometers and GPS-derived TEC, a sufficiently high EEP flux will eventually produce a detectable response, although for riometers the contribution of height-varying collision frequency makes the instrument less sensitive at the highest altitudes considered here. In general, riometers are more sensitive to the same EEP event occurring during the day than during the night, while subionospheric VLF shows the opposite relationship (i.e., more sensitive at night than during day). ΔvTEC changes are similar during the day and night. For subionospheric VLF the minimum detectable EEP energy of ∼150 keV (day) and ∼50 keV (night) is controlled by the differing reflection heights of VLF waves propagating under the undisturbed ionospheres. In general, the subionospheric VLF technique is more sensitive than the other two techniques for EEP with energies over 200 keV, responding to flux magnitudes two to three orders of magnitude smaller than detectable by a riometer. Detectable TEC changes only occur for unrealistically extreme monoenergetic fluxes.

[25] Figure 4 emphasizes the complex and nonlinear response of subionospheric VLF propagation to an ionospheric disturbance: both amplitude increases and decreases seen depending on the energy and flux magnitude of the EEP. Clearly, subionospheric VLF amplitude observations would be unsuitable for superposed epoch analysis, an approach which has proved valuable with riometers [e.g., *Longden et al.*, 2008; A. J. Kavanagh et al., Key features of >30 keV electron precipitation during high speed solar wind streams: A superposed epoch analysis, submitted to *Journal of Geophysical Research*, 2011]. In contrast, the phase changes are considerably better behaved with phase advances occurring for most EEP energy and flux conditions. Similar behavior has been reported previously in the subionospheric VLF amplitude and phase response to solar flares [e.g., *Thomson et al.*, 2005]. It is important to note that the received VLF broadcast is a summation of multiple modes after propagation in the Earth-ionosphere waveguide, and so the response of subionospheric VLF amplitude to EEP is highly dependent upon the combination of the transmitter and the receiver. Figure 5 presents estimates of amplitude response from two other VLF paths: NAA to Churchill (CHUR; Figure 5, top) and NAA to the Sodankylä Geophysical Observatory (SGO; Figure 5, bottom). The two paths are shown in Figure 2. Note that in the latter case we make use of the daytime ambient ionosphere and the disturbed ionosphere limits outlined by *Clilverd et al.* [2010] for consistency with later sections of the current study. Figures 4 and 5 show that the pattern of positive and negative subionospheric amplitude changes and their magnitude is different, even two similar paths (i.e., NDK to Churchill and NAA to Churchill). In addition, the minimum flux required for a measureable amplitude deviation varies strongly from path to path, especially for nighttime conditions.

4. EEP From the Radiation Belts

[26] As noted above, realistic EEP from the radiation belts is not well represented by idealized monoenergetic beams. We therefore consider the case of EEP with an energy spectrum provided by experimental measurements from the DEMETER spacecraft [*Clilverd et al.*, 2010]. While DEMETER primarily measured electrons in the drift loss cone, its measurements are more likely to be representative of the bounce loss cone than those of the trapped electron fluxes. The typical energy spectra presented by *Clilverd et al.* [2010] is, however, very similar in form to the energy spectra of the total tube content calculated from the ESA-SEE1 radiation belt model (not shown), providing additional confidence that this spectra is representative. In the current study we hold the energy spectrum constant and sweep through a range of EEP flux magnitudes. The model described in section 2 is used to determine the ionization rates and hence the altered electron density profiles from which the response

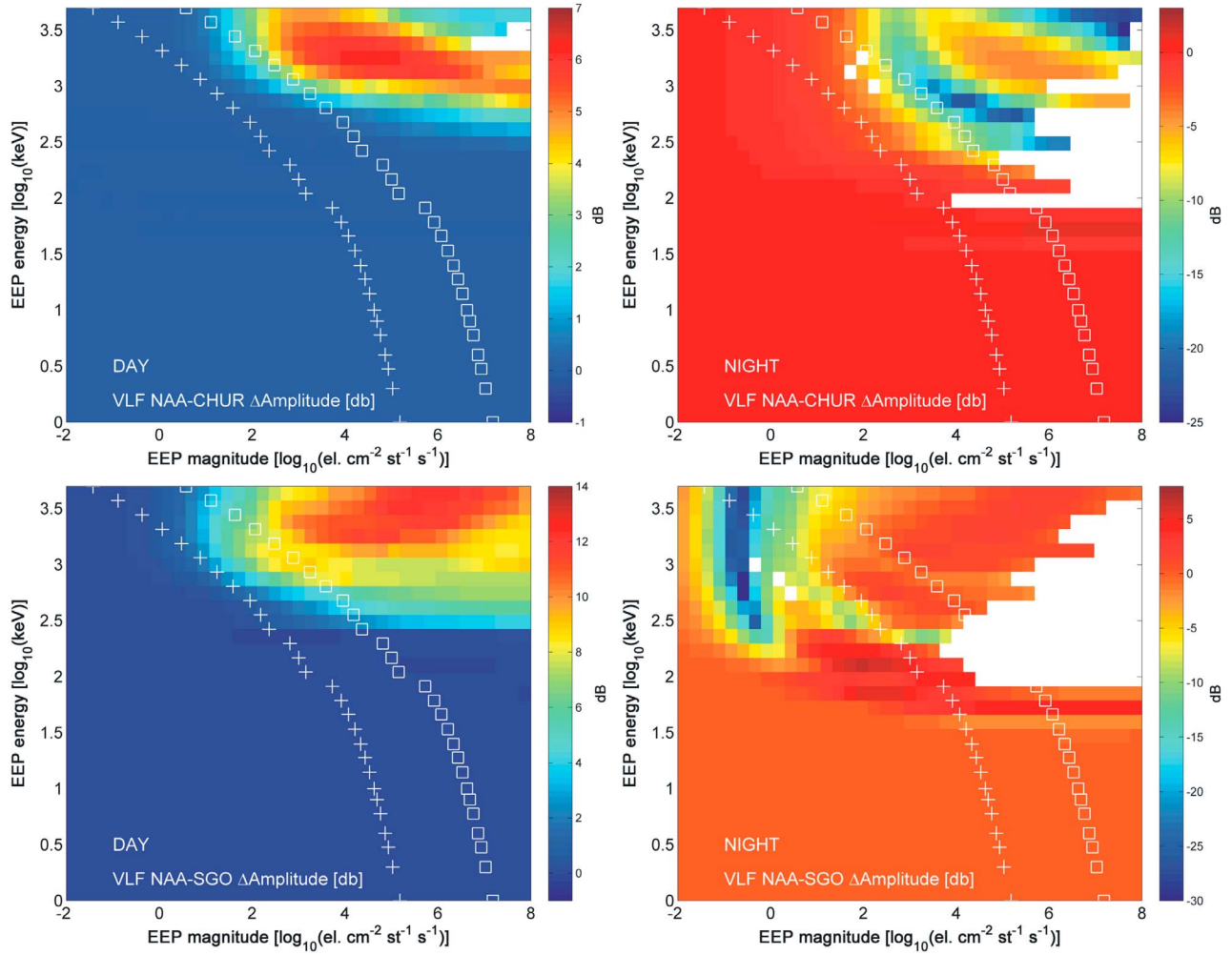

Figure 5. Same as Figure 4, but showing the response for two different subionospheric paths, (top) NAA to Churchill and (bottom) NAA to Sodankylä, as shown in Figure 1.

of the EEP sensing techniques is estimated. We assume the radiation belt EEP spans the energy range 30 keV to 3 MeV.

[27] Figure 6 shows the response of the three different techniques to radiation belt precipitation. The red line (at 1.3×10^6 electrons cm^{-2} sr^{-1} s^{-1}) is an indication of an extreme EEP flux case (again corresponding to the entire ESA-SEE1 model >30 keV tube population precipitated in 10 min). Figure 6 (top) displays the calculated response for riometers and GPS-derived TEC, while Figure 6 (bottom) shows the subionospheric VLF amplitude and phase changes for the path NDK to Churchill. Note that log scales are used for the *y*-axes of Figure 6 (top), while a linear scale is used for Figure 6 (bottom). Figure 6 demonstrates that a minimum detectable CNA change of ~0.1 dB requires a >30 keV EEP flux of $\sim 10^4$ electrons cm^{-2} st^{-1} s^{-1} for nighttime conditions when riometers are least sensitive, but the same response can be generated by a flux of only $\sim 5 \times 10^2$ electrons cm^{-2} st^{-1} s^{-1} for daytime conditions. A clearly detectable subionospheric VLF response (~0.5 dB in amplitude and ~10° in phase) is produced by nighttime flux of $\sim 1 \times 10^0$ electrons cm^{-2} st^{-1} s^{-1} and a daytime flux of $\sim 5 \times 10^1$ electrons cm^{-2} st^{-1} s^{-1}, i.e., 10,000 and 10 times lower respectively compared to riometers. Figure 6 suggests that riometers are likely to only respond to radiation belt fluxes during the largest EEP events, most likely during the peak activity during geomagnetic storms, and GPS derived vTEC is unlikely to be significantly disturbed by radiation belt EEP at all. Clearly, while the response of subionospheric VLF to EEP is potentially complex, it is reasonably sensitive to radiation belt EEP over a wide range of flux magnitudes and can provide a valuable remote sensing tool. *Clilverd et al.* [2010] showed that the path from NAA to SGO had a comparatively simple response for a sunlit path (as shown in Figure 7 of that paper), and thus EEP magnitudes could be extracted from the changing subionospheric VLF amplitudes. These authors use the Northern Hemisphere summer period, where the entire path was sunlit for the majority of the time and thus estimate EEP magnitudes for a ~160 day period. In the current study, we compare the observed subionospheric VLF amplitude difference from this 160 day period to the predicted riometer and TEC response given EEP fluxes consistent with those responsible for the VLF amplitude changes. Figure 7 (top) reproduces the NAA to SGO amplitude differences at 0230 UT reported by *Clilverd et al.* [2010]. Figure 7 (middle) shows the >30 keV EEP magnitudes derived from these observations using the

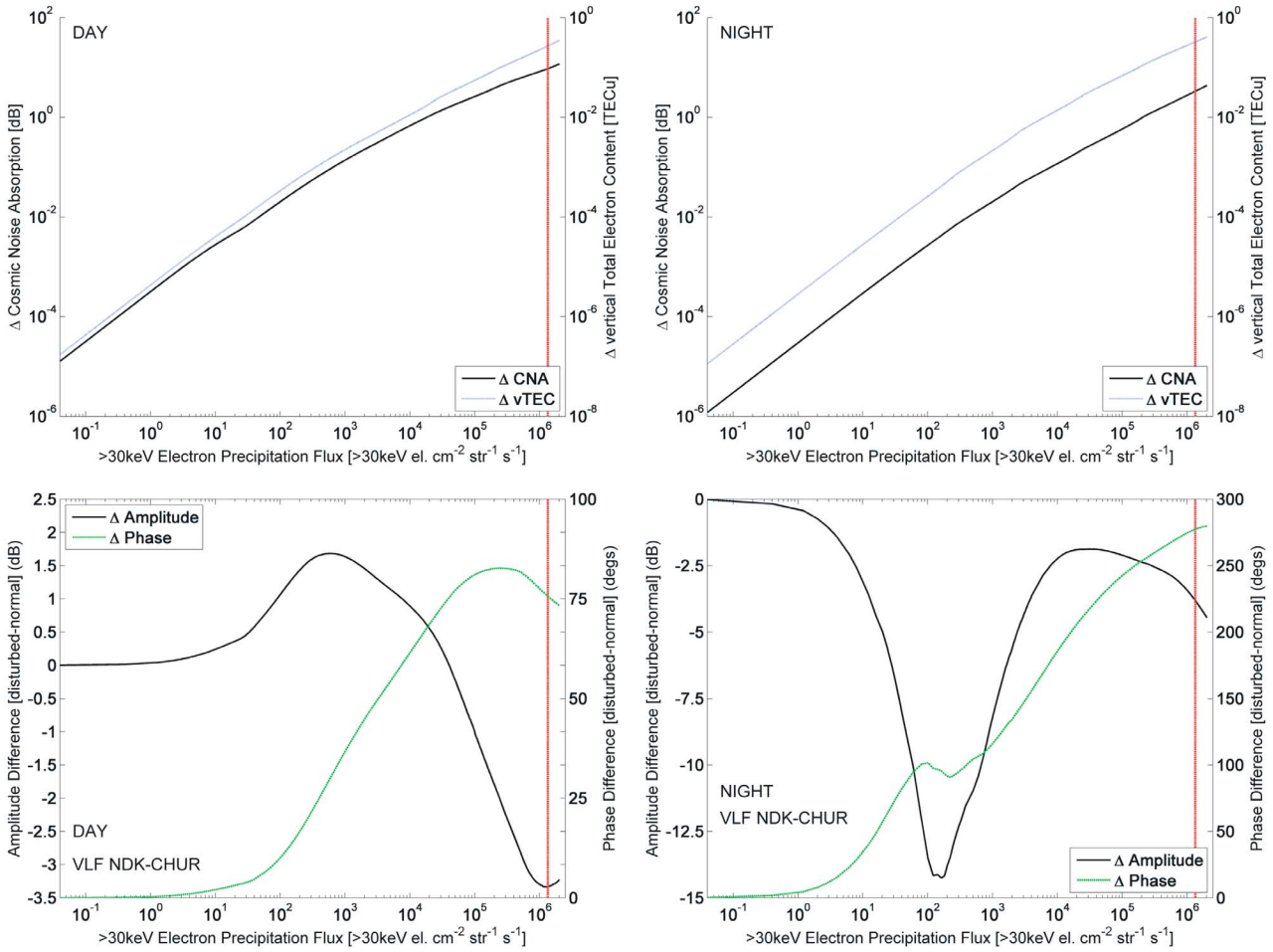

Figure 6. The varying response of the three EEP-sensing techniques to EEP with a energy spectrum that is realistic for precipitation from the radiation belts. (top) The calculated response for riometers and GPS-derived TEC and (bottom) the subionospheric VLF amplitude and phase changes. The red line represents an extreme EEP flux, where the entire ESA-SEE1 model tube population is precipitated in 10 min.

ionospheric model described in section 2.4. Periods where the VLF propagation would be influenced by solar protons impacting the polar ionosphere have been removed from Figure 7 (top) and the subsequent calculations. Figure 7 (bottom) shows the predicted response in ΔCNA and ΔvTEC produced by the estimated EEP fluxes. There is a clearly detectable change in riometer response during the periods of peak EEP fluxes, i.e., during storm times. The right-hand axis of Figure 7 (bottom) clearly demonstrates that there is no change in vTEC in the presence of stormtime high energy precipitation above the 0.1 TECu threshold required. It is therefore unlikely that riometers, or GPS-derived TEC can be used to measure radiation belt EEP in "normal" or "small" storm conditions, but that riometers will respond during the largest precipitation events.

5. EEP From Substorms

[28] Substorms generate EEP when the energy stored in the Earth's magnetotail is converted into particle heating and kinetic energy. It has long been recognized that substorms are accompanied by some level of particle precipitation through their association with brightening of auroral arcs. Recent papers have suggested that a very large fraction of the enhanced population energetic electrons (50–1000 keV) observed by geostationary satellites during substorms precipitate into the atmosphere. *Clilverd et al.* [2008] concluded that roughly 50% of the electrons injected near the LANL-97A satellite during a substorm on 1 March 2006 precipitated in the region near the satellite, and comparable EEP fluxes were reported by *Clilverd et al.* [2012] for another THEMIS detected-substorm occurring on 28 May 2010. Both of these studies combined the satellite measurements with observations from a riometer and subionospheric VLF instruments. In addition, *Watson et al.* [2011] examined GPS TEC measurements during substorms and reported vTEC changes of several TEC units associated with the substorm. By studying the apparent expansion of the precipitation region due to the substorm, they concluded that the bulk of the ΔvTEC change occurred at altitudes of approximately ~100 km, i.e., the vTEC was responding to the EEP and not the very considerable population of <1 keV electrons that also precipitate during substorms [*Mende et al.*, 2003]. In order to test this conclusion, we consider the response of riometers and subionospheric VLF during the events examined by *Clilverd et al.* [2008, 2012] and test whether the EEP

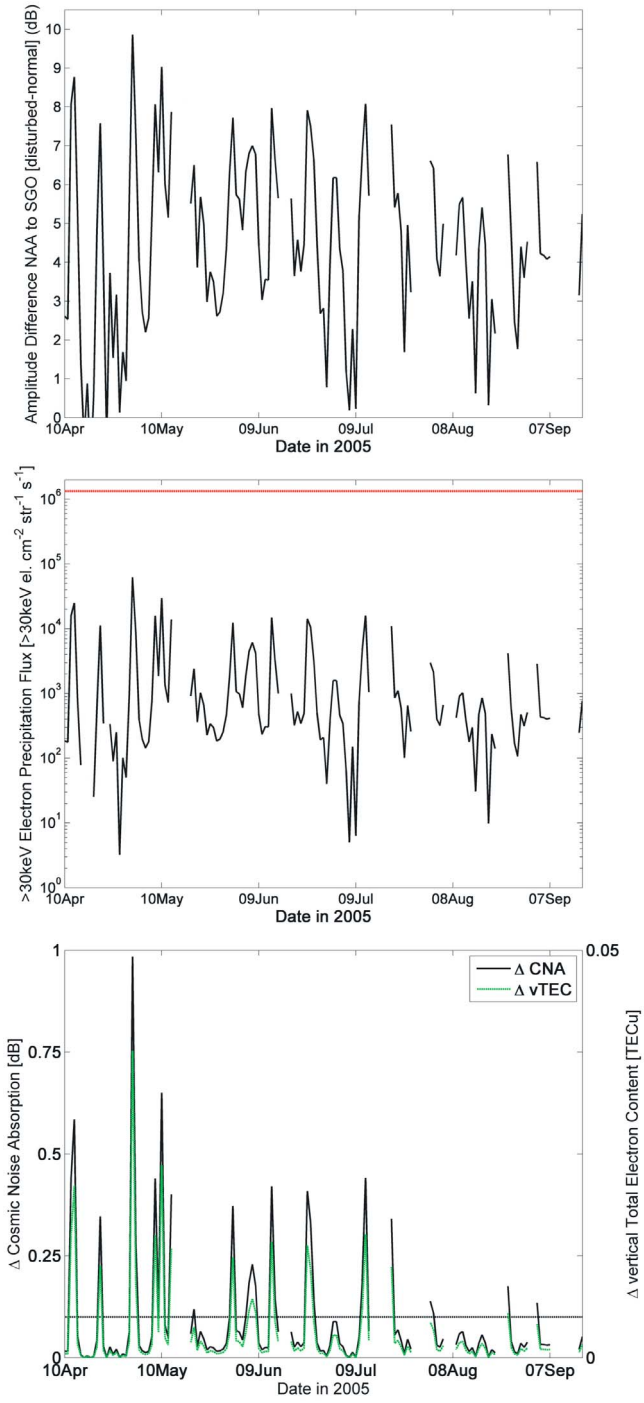

Figure 7. A comparison between (top) the variation of the NAA to SGO received amplitudes at 0230 UT in days 100–260 of 2005 (10 April to 17 September 2005), (middle) the >30 keV EEP flux determined from the NAA amplitudes, and (bottom) the response of a riometer and a GPS vTEC instrument sensing the same ionospheric disturbance as the subionospheric VLF instrument. The red line represents an extreme EEP flux, where the entire ESA-SEE1 model tube population is precipitated in 10 min. The horizontal black line in Figure 7 (bottom) is an indication of the lowest riometer detection sensitivity.

Table 1. Summary of Ground-Based EEP Instrument Responses During Two Substorms Reported by *Clilverd et al.* [2008, 2012][a]

Event	ΔCNA	ΔVLF	ΔvTEC	EEP
1 March 2006				
Observed experimental	2.9 dB	−15 dB	–	–
Calculation results	2.9 dB	−9 dB	3.1 TECu	0.8×10^7
	5.4 dB	−15 dB	4.2 TECu	2.6×10^7
28 May 2010				
Observed experimental	3.2 dB	210°	–	–
Calculation results	3.2 dB	210°	4.8 TUCu	1.1×10^7

[a]Beneath the experimental observations are the calculated results for the modeling of each of the two events, as described in the text. The EEP values listed are >30 keV electron fluxes with units of electrons cm^{-2} st^{-1} s^{-1}.

striking the atmosphere below 150 km can explain the reported vTEC changes.

[29] *Clilverd et al.* [2008, 2012] modeled the substorm signature in ground-based data using 30 keV–2.5 MeV EEP spectra derived from satellite measurements (LANL-97A and THEMIS, respectively). In order to model the two substorms reported in those papers, we expand the energy spectra to encompass EEP with energies from 1 keV. The EEP flux at 1 keV is set at 3×10^9 electrons cm^{-2} st^{-1} s^{-1} taken from FAST measurements reported during a substorm which was said to be "fairly typical" [*Mende et al.*, 2003, Figure 4a]. The flux at 1 keV is joined smoothly using a power law to the 30 keV–2.5 MeV EEP spectra described above.

[30] Table 1 summarizes the results of this modeling. We list the observed riometer response at Macquarie Island (54.5°S, 158.9°E, $L = 5.4$) and the observed subionospheric VLF response at the Australian Antarctic Division station Casey (66.3°S, 110.5°E, $L > 999$). We use the signal measured at Casey from the powerful U.S. Navy transmitter NWC, located in western Australia. The first of the two substorms occurred on 1 March 2006; the peak riometer ΔCNA was 2.9 dB, associated with a 15 dB decrease in the amplitude of NWC measured at Casey. We estimate that this VLF subionospheric amplitude decrease is produced from a >30 keV EEP flux of 2.6×10^7 electrons cm^{-2} st^{-1} s^{-1} [*Clilverd et al.*, 2008] which would lead to a riometer ΔCNA of 5.4 dB. In contrast, the model suggests that the observed riometer ΔCNA of 2.9 dB could be produced from a >30 keV EEP flux of 0.8×10^7 electrons cm^{-2} st^{-1} s^{-1} which would lead to a decrease in the VLF amplitude from NWC of 9 dB at Casey. The two different predicted EEP spectra for these situations are shown in Figure 8. Case 1 of 1 March 2006 represents the predicted spectra from the riometer measurement (ΔCNA = 2.9 dB, first "Calculation Results" line in Table 1) while Case 2 represents the predicted spectra from the subionospheric VLF measurement (ΔVLF of −15 dB, second "Calculation Results" line in Table 1) Clearly, there is some uncertainty in the EEP magnitude, which may come from the high variability of winter nighttime amplitudes, but the two EEP fluxes differ only by a factor of three. Both the potential modeling solutions lead to significant predicted ΔvTEC, 3.1 and 4.2 TECu, respectively.

[31] The second of the two substorms occurred on 28 May 2010, after the Casey subionospheric VLF receiver was upgraded such that phase changes could be determined.

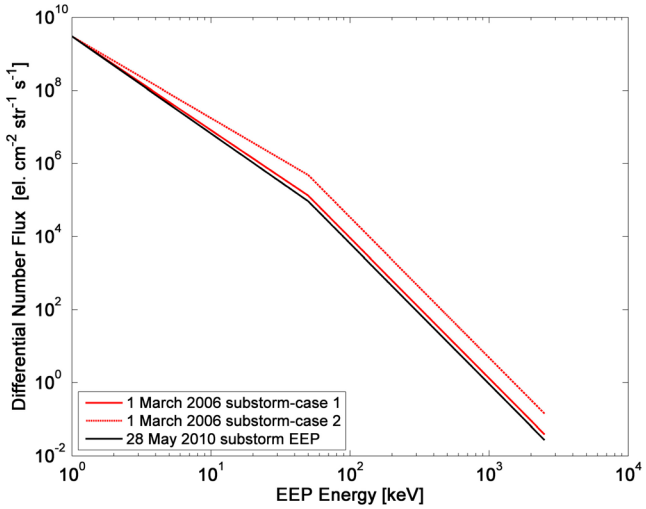

Figure 8. Comparison between the substorm-associated differential EEP fluxes for the calculation cases given in Table 1. Case 1 of 01 March 2006 is the first "Calculation results" line (i.e., 2.9 dB) of Table 1, while Case 2 is for the second line (5.4 dB).

Clilverd et al. [2012] report a riometer ΔCNA of 3.2 dB, associated with a 210° phase advance of the signal from NWC measured at Casey. They argued that the phase changes should provide a more accurate indication of the EEP because the NWC-Casey quiet day phase variations are more consistent than the quiet day amplitude variations during the nighttime in the winter months. We estimate that this VLF subionospheric phase increase is produced from a >30 keV EEP flux of 1.1×10^7 electrons cm^{-2} st^{-1} s^{-1} which leads to a riometer ΔCNA of 3.2 dB and ΔvTEC of 4.8 TECu. The predicted differential EEP flux for this situation is shown in Figure 8. In this case there is very good agreement between the EEP flux predicted from both the riometer and the subionospheric phase for this substorm. Our model predicts that an EEP flux of 1.1×10^7 electrons cm^{-2} st^{-1} s^{-1} produces ΔvTEC of 4.8 TECu, which is in the upper range reported by *Watson et al.* [2011, Figure 12].

[32] The conclusion of *Watson et al.* [2011] that a significant fraction of the substorm-associated ΔvTEC changes occur in the *D* and *E* regions is supported by our calculations. However, we find that only about one-third to one-half of the ΔvTEC changes are due to increased ionization at altitudes below 120 km altitude, with the remainder of the change due to ionization at higher altitudes.

6. Discussion

[33] While we have shown that the response of subionospheric VLF to EEP is complicated, we have also shown that it is reasonably sensitive to a wide range of flux magnitudes and can provide a valuable remote sensing tool. For any given transmitter to receiver great circle path the response of the received amplitude to varying EEP conditions can be an increase or a decrease in amplitude. However, under similar propagation conditions, the received phase is more likely to show quasi-linear increases as EEP flux magnitudes increase. Thus VLF phase measurements are potentially more useful than amplitude measurements in determining EEP characteristics. The main caveat associated with this statement is associated with time-scales. The VLF phase measurement is more difficult to make consistently over long periods of time in comparison with VLF amplitude. Several factors contribute to this difficulty: phase locking to unstable transmissions, non-integer broadcast frequencies, and the lack of transmitter phase consistency between transmitter maintenance cycles or transmitter off-periods. While some VLF transmitters appear to have oscillators which are locked to GPS or atomic clocks and broadcast at the stated frequency, others appear to be offset from the nominal frequency; an example of this is the VLF transmitter near Ebino, Japan, which has a nominal operational frequency of 22.2 kHz but produces better quality amplitude and phase observations if the GPS-locked receiver is set to 22200.1175 Hz. In addition, most operational transmitters stop broadcasting once a week for a several hour period during which maintenance is undertaken, leading to unpredictable leaps in phase. In principle it is possible to indentify and compensate for many of these issues, but the longer the period of study the more difficult it is to positively identify phase variations that have been produced by EEP. When the perturbations caused by EEP are only minutes or hours long, then VLF phase is a very good investigative tool. However, if an EEP event lasts for more that a day then phase analysis can become contaminated by the instrument effects listed above, and great care needs to be taken. For events lasting 5–10 days, such as EEP from the radiation belts, the analysis of VLF phase is likely to be very difficult. These difficulties could be mitigated if complementary phase information was recorded close to the transmitters, or if official information about the phase was transmitted.

[34] The modeling results presented in section 4 suggest that, considering the realistic energy spectra and flux range, riometers will only respond to EEP with energies >30 keV during the largest radiation belt storms, and even then not particularly strongly. Riometers can respond to EEP events that include a significant population of electron energies <30 keV and that includes substorm events. Such electrons deposit the majority of their energy above the *D* region (i.e., above ~90 km) around the altitude range where riometer absorption peaks.

[35] GPS TEC-measurements are not sensitive enough to monitor precipitation from the radiation belts, and have only a small response to substorms. It should be noted, however, that GPS instruments can produce more significant vTEC changes during EEP events if there are a significant population of electrons with energies <30 keV. For soft EEP events (5–30 keV) there is only a small variation in riometer CNA, no effect on VLF propagation, but significant changes in vTEC. Watson called this "auroral" precipitation [*Watson et al.*, 2011].

7. Summary and Conclusions

[36] In order to make best use of the opportunities provided by upcoming space missions such as the Radiation Belt Storm Probes, we have determined the response of three different techniques to different energetic electron precipitation (EEP) characteristics. All of the techniques selected

have extensive ground-based instrumentation networks and are used to study EEP. Here we focused upon subionospheric radiowave propagation measurements (VLF), riometer absorption measurements (CNA), and GPS produced total electron content (vTEC). All of the three electromagnetic remote sensing techniques are comparatively low cost, as the "transmitter" is either funded independently of the science goal, as in the case of the subionospheric VLF and GPS satellite networks, or is a natural source, as in the case of riometers. In our study we contrasted the predicted sensitivity and responses of these instruments to idealized monoenergetic beams of precipitating electrons, and precipitating spectra derived from in situ experiments which represent energetic electron precipitation from the radiation belts and during substorms.

[37] For the monoenergetic beam case we found that riometers are more sensitive to the same EEP event occurring during the day than during the night, while subionospheric VLF showed the opposite relationship. ΔvTEC changes were similar for both day and night ionospheric conditions. In general, the subionospheric VLF technique is more sensitive than the other two techniques for EEP with energies over 200 keV, responding to flux magnitudes two to three orders of magnitude smaller than that detectable by a riometer. Detectable TEC changes only occurred for extreme monoenergetic fluxes, which appear to be beyond the levels one expects in reality.

[38] For the radiation belt EEP case clearly detectable subionospheric VLF responses are produced by daytime fluxes that are $\sim$10 times lower than required for riometers, while nighttime fluxes can be 10,000 times lower that that required for a riometer viewing the same event, and still produce a detectable response in the subionospheric VLF observations. We found that riometers are likely to only respond to radiation belt fluxes during the largest EEP events. In contrast, GPS derived vTEC is unlikely to be significantly disturbed by radiation belt EEP at all. It should be noted that this conclusion refers to EEP with energies >30 keV using an experimentally derived EEP spectrum; riometers and GPS instruments could produce more significant ΔCNA and vTEC changes during EEP events if there were a significant population of electrons with energies <30 keV.

[39] In the case of EEP during substorms, the responses predicted for the riometer absorption and the subionospheric VLF technique are both significant and clearly detectable. This is also true for the ΔvTEC, which is at a clearly detectable level of $\sim$3–4 TECu. Half of the vTEC changes in substorms are due to increased ionization below 120 km altitude, which is consistent with the conclusions of a recent study [*Watson et al.*, 2011] who speculated that substorm-associated vTEC changes were likely to be occurring in the *D* and *E* regions of the ionosphere.

[40] **Acknowledgments.** C.J.R. would like to thank Lynette Finnie of Dunedin for her support. C.J.R. was supported by the New Zealand Marsden Fund. The research leading to these results has received funding from the European Union Seventh Framework Programme (FP7/2007–2013) under grant agreement 263218. A.J.K. was supported by the UK Science and Technology Facilities Council (grant ST/G002401/1), C.E.J.W. by the Canadian Space Agency, and P.T.V. by the Academy of Finland through the project 136225/SPOC (Significance of Energetic Electron Precipitation to Odd Hydrogen, Ozone, and Climate).

References

Alfonsi, L., et al. (2008), Probing the high latitude ionosphere from ground-based observations: The state of current knowledge and capabilities during IPY (2007–2009), *J. Atmos. Sol. Terr. Phys.*, *70*(18), 2293–2308, doi:10.1016/j.jastp.2008.06.013.

Anderson, D. N., M. Mendillo, and B. Herniter (1987), A semi-empirical low-latitude ionospheric model, *Radio Sci.*, *22*(2), 292–306, doi:10.1029/RS022i002p00292.

Arikan, F., C. B. Erol, and O. Arikan (2003), Regularized estimation of vertical total electron content from Global Positioning System data, *J. Geophys. Res.*, *108*(A12), 1469, doi:10.1029/2002JA009605.

Barr, R., D. L. Jones, and C. J. Rodger (2000), ELF and VLF radio waves, *J. Atmos. Sol. Terr. Phys.*, *62*(17–18), 1689–1718, doi:10.1016/S1364-6826(00)00121-8.

Brasseur, G., and S. Solomon (2005), *Aeronomy of the Middle Atmosphere*, 3rd ed., Springer, Dordrecht, Netherlands.

Clilverd, M. A., N. R. Thomson, and C. J. Rodger (1999), Sunrise effects on VLF signals propagated over a long north–south path, *Radio Sci.*, *34*(4), 939–948, doi:10.1029/1999RS900052.

Clilverd, M. A., C. J. Rodger, and T. Ulich (2006), The importance of atmospheric precipitation in storm-time relativistic electron flux drop outs, *Geophys. Res. Lett.*, *33*, L01102, doi:10.1029/2005GL024661.

Clilverd, M. A., et al. (2008), Energetic electron precipitation during substorm injection events: High-latitude fluxes and an unexpected midlatitude signature, *J. Geophys. Res.*, *113*, A10311, doi:10.1029/2008JA013220.

Clilverd, M. A., et al. (2009), Remote sensing space weather events: Antarctic-Arctic Radiation-belt (Dynamic) Deposition-VLF Atmospheric Research Konsortium network, *Space Weather*, *7*, S04001, doi:10.1029/2008SW000412.

Clilverd, M. A., C. J. Rodger, R. J. Gamble, T. Ulich, T. Raita, A. Seppälä, J. C. Green, N. R. Thomson, J.-A. Sauvaud, and M. Parrot (2010), Ground-based estimates of outer radiation belt energetic electron precipitation fluxes into the atmosphere, *J. Geophys. Res.*, *115*, A12304, doi:10.1029/2010JA015638.

Clilverd, M. A., C. J. Rodger, I. J. Rae, J. B. Brundell, N. R. Thomson, N. Cobbett, P. T. Verronen, and F. W. Menk (2012), Combined THEMIS and ground-based observations of a pair of substorm-associated electron precipitation events, *J. Geophys. Res.*, *117*, A02313, doi:10.1029/2011JA016933.

Detrick, D. L., and T. J. Rosenberg (1990), A phased-array radiowave imager for studies of cosmic noise absorption, *Radio Sci.*, *25*, 325–338, doi:10.1029/RS025i004p00325.

Ferguson, J. A., and F. P. Snyder (1990), Computer programs for assessment of long wavelength radio communications, version 1.0, *Tech. Doc., 1773*, Nav. Ocean Syst. Cent., San Diego, Calif.

Friedel, R. H. W., G. D. Reeves, and T. Obara (2002), Relativistic electron dynamics in the inner magnetosphere—A review, *J. Atmos. Sol. Terr. Phys.*, *64*(2), 265–282, doi:10.1016/S1364-6826(01)00088-8.

Friedrich, M., M. Harrich, K. Torkar, and P. Stauning (2002), Quantitative measurements with wide-beam riometers, *J. Atmos. Sol. Terr. Phys.*, *64*, 359–365, doi:10.1016/S1364-6826(01)00108-0.

Goldberg, R. A., C. H. Jackman, J. R. Barcus, and F. Søraas (1984), Nighttime auroral energy deposition in the middle atmosphere, *J. Geophys. Res.*, *89*(A7), 5581–5596, doi:10.1029/JA089iA07p05581.

Green, J. C., T. G. Onsager, T. P. O'Brien, and D. N. Baker (2004), Testing loss mechanisms capable of rapidly depleting relativistic electron flux in the Earth's outer radiation belt, *J. Geophys. Res.*, *109*, A12211, doi:10.1029/2004JA010579.

Hess, W. N. (1968), *The Radiation Belt and Magnetosphere*, Blaisdell, London.

Horne, R. B. (2002), The contribution of wave-particle interactions to electron loss and acceleration in the Earth's radiation belts during geomagnetic storms, in *The Review of Radio Science, 1999–2002*, edited by W. R. Stone, pp. 801–828, IEEE Press, Piscataway, N. J.

Jayachandran, P. T., et al. (2009), Canadian High Arctic Ionospheric Network (CHAIN), *Radio Sci.*, *44*, RS0A03, doi:10.1029/2008RS004046.

Krishnaswamy, S., D. L. Detrick, and T. J. Rosenberg (1985), The inflection point method of determining riometer quiet day curves, *Radio Sci.*, *20*, 123–136, doi:10.1029/RS020i001p00123.

Little, C. G., and H. Leinbach (1959), The riometer—A device for the continuous measurement of ionospheric absorption, *Proc. IRE*, *47*, 315–320, doi:10.1109/JRPROC.1959.287299.

Longden, N., M. H. Denton, and F. Honary (2008), Particle precipitation during ICME-driven and CIR-driven geomagnetic storms, *J. Geophys. Res.*, *113*, A06205, doi:10.1029/2007JA012752.

Lorentzen, K. R., M. D. Looper, and J. B. Blake (2001), Relativistic electron microbursts during the GEM storms, *Geophys. Res. Lett.*, *28*(13), 2573–2576, doi:10.1029/2001GL012926.

Mende, S. B., C. W. Carlson, H. U. Frey, L. M. Peticolas, and N. Østgaard (2003), FAST and IMAGE-FUV observations of a substorm onset, *J. Geophys. Res.*, *108*(A9), 1344, doi:10.1029/2002JA009787.

Mendillo, M. (2006), Storms in the ionosphere: Patterns and processes for total electron content, *Rev. Geophys.*, *44*, RG4001, doi:10.1029/2005RG000193.

Millan, R. M., and the BARREL Team (2011), Understanding relativistic electron losses with BARREL, *J. Atmos. Sol. Terr. Phys.*, *73*, 1425–1434, doi:10.1016/j.jastp.2011.01.006.

Millan, R. M., and R. M. Thorne (2007), Review of radiation belt relativistic electron losses, *J. Atmos. Sol. Terr. Phys.*, *69*, 362–377, doi:10.1016/j.jastp.2006.06.019.

Morley, S. K., R. H. W. Friedel, E. L. Spanswick, G. D. Reeves, J. T. Steinberg, J. Koller, T. Cayton, and E. Noveroske (2010), Dropouts of the outer electron radiation belt in response to solar wind stream interfaces: Global Positioning System observations, *Proc. R. Soc. A*, *466*(2123), 3329–3350, doi:10.1098/rspa.2010.0078.

Newnham, D. A., P. J. Espy, M. A. Clilverd, C. J. Rodger, A. Seppälä, D. J. Maxfield, P. Hartogh, K. Holmén, and R. B. Horne (2011), Direct observations of nitric oxide produced by energetic electron precipitation into the Antarctic middle atmosphere, *Geophys. Res. Lett.*, *38*, L20104, doi:10.1029/2011GL048666.

Nyland, I. (2007), A comparison study between cosmic noise absorption and flux of precipitating energetic electrons, MSc thesis, Univ. of Bergen, Bergen, Norway.

Picone, J. M., A. E. Hedin, D. P. Drob, and A. C. Aikin (2002), NRLMSISE-00 empirical model of the atmosphere: Statistical comparisons and scientific issues, *J. Geophys. Res.*, *107*(A12), 1468, doi:10.1029/2002JA009430.

Randall, C. E., V. L. Harvey, C. S. Singleton, S. M. Bailey, P. F. Bernath, M. Codrescu, H. Nakajima, and J. M. Russell III (2007), Energetic particle precipitation effects on the Southern Hemisphere stratosphere in 1992–2005, *J. Geophys. Res.*, *112*, D08308, doi:10.1029/2006JD007696.

Rees, M. H. (1989), *Physics and Chemistry of the Upper Atmosphere*, Cambridge Univ. Press, Cambridge, U. K., doi:10.1017/CBO9780511573118.

Reeves, G. D., K. L. McAdams, R. H. W. Friedel, and T. P. O'Brien (2003), Acceleration and loss of relativistic electrons during geomagnetic storms, *Geophys. Res. Lett.*, *30*(10), 1529, doi:10.1029/2002GL016513.

Reeves, G. D., A. Chan, and C. Rodger (2009), New directions for radiation belt research, *Space Weather*, *7*, S07004, doi:10.1029/2008SW000436.

Rodger, C. J., O. A. Molchanov, and N. R. Thomson (1998), Relaxation of transient ionization in the lower ionosphere, *J. Geophys. Res.*, *103*, 6969–6975, doi:10.1029/98JA00016.

Rodger, C. J., M. A. Clilverd, N. R. Thomson, R. J. Gamble, A. Seppälä, E. Turunen, N. P. Meredith, M. Parrot, J.-A. Sauvaud, and J.-J. Berthelier (2007), Radiation belt electron precipitation into the atmosphere: Recovery from a geomagnetic storm, *J. Geophys. Res.*, *112*, A11307, doi:10.1029/2007JA012383.

Rodger, C. J., M. A. Clilverd, A. Seppälä, N. R. Thomson, R. J. Gamble, M. Parrot, J.-A. Sauvaud, and T. Ulich (2010), Radiation belt electron precipitation due to geomagnetic storms: Significance to middle atmosphere ozone chemistry, *J. Geophys. Res.*, *115*, A11320, doi:10.1029/2010JA015599.

Rozanov, E., L. Callis, M. Schlesinger, F. Yang, N. Andronova, and V. Zubov (2005), Atmospheric response to NOy source due to energetic electron precipitation, *Geophys. Res. Lett.*, *32*, L14811, doi:10.1029/2005GL023041.

Seppälä, A., M. A. Clilverd, and C. J. Rodger (2007), NOx enhancements in the middle atmosphere during 2003–2004 polar winter: Relative significance of solar proton events and the aurora as a source, *J. Geophys. Res.*, *112*, D23303, doi:10.1029/2006JD008326.

Seppälä, A., C. E. Randall, M. A. Clilverd, E. Rozanov, and C. J. Rodger (2009), Geomagnetic activity and polar surface air temperature variability, *J. Geophys. Res.*, *114*, A10312, doi:10.1029/2008JA014029.

Skone, S. H. (2001), The impact of magnetic storms on GPS receiver performance, *J. Geod.*, *75*, 457–468, doi:10.1007/s001900100198.

Thomson, N. R., and W. M. McRae (2009), Nighttime ionospheric *D* region: Equatorial and nonequatorial, *J. Geophys. Res.*, *114*, A08305, doi:10.1029/2008JA014001.

Thomson, N. R., C. J. Rodger, and M. A. Clilverd (2005), Large solar flares and their ionospheric *D* region enhancements, *J. Geophys. Res.*, *110*, A06306, doi:10.1029/2005JA011008.

Thomson, N. R., C. J. Rodger, and M. A. Clilverd (2011), Daytime *D* region parameters from long-path VLF phase and amplitude, *J. Geophys. Res.*, *116*, A11305, doi:10.1029/2011JA016910.

Thorne, R. M. (2010), Radiation belt dynamics: The importance of wave-particle interactions, *Geophys. Res. Lett.*, *37*, L22107, doi:10.1029/2010GL044990.

Turunen, E., P. T. Verronen, A. Seppälä, C. J. Rodger, M. A. Clilverd, J. Tamminen, C.-F. Enell, and T. Ulich (2009), Impact of different energies of precipitating particles on NOx generation in the middle and upper atmosphere during geomagnetic storms, *J. Atmos. Sol. Terr. Phys.*, *71*, 1176–1189, doi:10.1016/j.jastp.2008.07.005.

Ukhorskiy, A. Y., B. J. Anderson, P. C. Brandt, and N. A. Tsyganenko (2006), Storm time evolution of the outer radiation belt: Transport and losses, *J. Geophys. Res.*, *111*, A11S03, doi:10.1029/2006JA011690.

Vampola, A. L. (1997), Outer zone energetic electron environment update, in *Conference on the High Energy Radiation Background in Space*, edited by P. H. Solomon, pp. 101–104, NASA Cent. for AeroSpace Inf., Linthicum Heights, Md.

Van Allen, J. A. (1997) Energetic particles in the Earth's external magnetic field, in *Discovery of the Magnetosphere*, *Hist. Geophys. Ser.*, vol. 7, edited by C. S. Gillmor and J. R. Spreiter, pp. 235–251, AGU, Washington, D. C., doi:10.1029/HG007p0235.

Van Allen, J. A., and L. A. Frank (1959), Radiation measurements to 658,300 km. with *Pioneer IV*, *Nature*, *184*, 219–224, doi:10.1038/184219a0.

Verronen, P. T., A. Seppälä, M. A. Clilverd, C. J. Rodger, E. Kyrölä, C.-F. Enell, T. Ulich, and E. Turunen (2005), Diurnal variation of ozone depletion during the October–November 2003 solar proton events, *J. Geophys. Res.*, *110*, A09S32, doi:10.1029/2004JA010932.

Verronen, P. T., C. J. Rodger, M. A. Clilverd, and S. Wang (2011), First evidence of mesospheric hydroxyl response to electron precipitation from the radiation belts, *J. Geophys. Res.*, *116*, D07307, doi:10.1029/2010JD014965.

Watson, C., P. T. Jayachandran, E. Spanswick, E. F. Donovan, and D. W. Danskin (2011), GPS TEC technique for observation of the evolution of substorm particle precipitation, *J. Geophys. Res.*, *116*, A00I90, doi:10.1029/2010JA015732.

M. A. Clilverd, British Antarctic Survey, National Environment Research Council, High Cross, Madingley Road, Cambridge CB3 0ET, UK.

A. J. Kavanagh, Department of Physics, Lancaster University, Lancaster LA1 4WA, UK.

T. Raita, Sodankylä Geophysical Observatory, University of Oulu, FI-99600 Sodankylä, Finland.

C. J. Rodger, Department of Physics, University of Otago, PO Box 56, Dunedin 9016, New Zealand. (crodger@physics.otago.ac.nz)

P. T. Verronen, Finnish Meteorological Institute, PO Box 503, FI-00101 Helsinki, Finland.

C. E. J. Watt, Department of Physics, University of Alberta, Edmonton, AB T6G 2E1, Canada.